

Eccentric black hole-neutron star mergers: effects of black hole spin and equation of state

William E. East¹, Frans Pretorius¹, and Branson C. Stephens²

¹*Department of Physics, Princeton University, Princeton, NJ 08544, USA.*

²*Center for Gravitation and Cosmology, University of Wisconsin-Milwaukee, Milwaukee, WI 53211, USA.*

There is a high level of interest in black hole-neutron star binaries, not only because their mergers may be detected by gravitational wave observatories in the coming years, but also because of the possibility that they could explain a class of short duration gamma-ray bursts. We study black hole-neutron star mergers that occur with high eccentricity as may arise from dynamical capture in dense stellar regions such as nuclear or globular clusters. We perform general relativistic simulations of binaries with a range of impact parameters, three different initial black hole spins (zero, aligned and anti-aligned with the orbital angular momentum), and neutron stars with three different equations of state. We find a rich diversity across these parameters in the resulting gravitational wave signals and matter dynamics, which should also be reflected in the consequent electromagnetic emission. Before tidal disruption, the gravitational wave emission is significantly larger than perturbative predictions suggest for periapsis distances close to effective innermost stable separations, exhibiting features reflecting the zoom-whirl dynamics of the orbit there. Guided by the simulations, we develop a simple model for the change in orbital parameters of the binary during close encounters. Depending upon the initial parameters of the system, we find that mass transfer during non-merging close encounters can range from essentially zero to a sizable fraction of the initial neutron star mass. The same holds for the amount of material outside the black hole post-merger, and in some cases roughly half of this material is estimated to be unbound. We also see that non-merging close encounters generically excite large oscillations in the neutron star that are qualitatively consistent with f -modes.

I. INTRODUCTION

It is important to understand mergers of black holes (BHs) and neutron stars (NSs) not only because they are a chief source for ground-based gravitational wave (GW) detectors (such as LIGO [1]) but also because they may be accompanied by a diverse range of electromagnetic (EM) and neutrino emission. One of the more interesting possibilities in this regard is that BH-NS mergers may be progenitors of a fraction of observed short-hard gamma-ray bursts (sGRBs) [2–4]. Furthermore, existing and planned wide-field survey telescopes such as PTF [5], Pan-STARRS [6], and LSST [7] are beginning to observe and classify fainter EM transient events, some of which are expected to be produced in BH-NS mergers from a variety of mechanisms (see [8] for a recent, detailed exploration of the possibilities). Coincident observation of these EM events with a gravitational wave signal from a binary coalescence would provide a wealth of additional information about the system beyond any individual observation, provided we have a good understanding of how to map the particular observations to the underlying astrophysical processes governing the merger.

The great diversity in sGRBs hints at the possibility that there will be a corresponding diversity in the associated GW and EM signals, and motivates the exploration of all viable channels for binary compact (BCO) mergers. BCOs may form through the evolution of primordial binaries or through dynamical capture in dense stellar systems, such as nuclear or globular clusters. BCOs formed through the latter channel, which could merge with non-negligible eccentricity, are the focus of this work, which is a follow up of a first study of dynamical capture BH-

NS evolution using full general relativistic hydrodynamics [9]. Before delving into the details, we briefly summarize the motivation for studying this class of BCO; see [9] and a related study on eccentric NS-NS mergers [10] for more discussion. In contrast, most studies of BH-NS mergers to date have focused on the quasi-circular inspiral case; see [11] for a review of these efforts.

A chance close encounter of a BH and NS in a stellar cluster could result in a bound system if the energy loss due to GW emission is sufficiently large. (Tidal interaction with the NS is also a source of energy loss, though to leading order the total cross section for capture is dominated by the GW emission.) Due to gravitational focusing, a sizable fraction of binding encounters will result in highly eccentric binaries that merge within a few orbits of the initial encounter—in fact, for the 4:1 BH to NS mass ratio systems studied here, roughly 20% of such encounters are “direct collisions,” merging on the first encounter.

At first glance it may seem that such encounters would be too rare to be of any relevance as possible GW or EM transient sources; however, recent studies have suggested otherwise. In [12] estimates of BH-BH encounters in galactic nuclear clusters suggest Advanced LIGO rates of $O(1-10^3)$ per year, while in [13] (following earlier work in [14–16]) it was argued that direct capture NS-NS mergers in globular clusters could account for a sizable fraction of observed sGRBs. Scaling this latter study’s results to BH-NS systems implies dynamical capture event rates of $O(10-10^2) \text{ yr}^{-1} \text{ Gpc}^{-3}$. To estimate Advanced LIGO detection rates would require full templates for these events, which we relegate to a future study; however, in [17] the signal-to-noise ratio was computed using

post-Newtonian based models of the early stages of the mergers, which showed that a subset (depending upon the component masses) could be observed out to several hundred Mpc, even excluding the final stages of the merger in the templates.

Though far from conclusive, there is also observational evidence for multiple sGRB progenitors, which could in part be due to dynamical capture versus primordial mergers. Of sGRBs with identified host galaxies, $\sim 25\%$ have offsets of $\gtrsim 15$ kpc from their hosts [18]. This subset of sGRBs with large offsets would be consistent with kicked, primordially formed BCOs or with dynamically formed binaries in GCs. The latter may be preferred for the largest offsets [19], especially if primordial BCOs experience weak kicks [20]. Analysis of X-ray afterglows observed by Swift/XRT suggests that different progenitors may be responsible for sGRBs with and without extended emission [21]; again, one possible explanation is dynamical capture (leading to extended emission) vs. primordial. There has also been a claim that a very-high-energy gamma-ray source observed in Terzan 5 may in fact be the remnant of a BCO merger-powered sGRB [22]; if true, this would support the claim that dense cluster environments can be significant sources of BCO mergers.

It has also been suggested that some merging NS-NS or BH-NS binaries are actually part of a coeval or dynamically formed triple [23]. The tertiary (for example a white dwarf) drives the binary to high eccentricities through a Kozai resonance, resulting in a faster merger time. Though dynamically different from direct capture two body systems, in Kozai-accelerated evolution the merger itself could take place with significant eccentricity [24] and have comparable behavior at late times to the systems studied here.

Merging with moderate to high eccentricity could have significant effects on all the GW and EM observables from the event. In contrast to a low eccentricity inspiral, the GWs are emitted primarily around periapsis, resulting in waveforms that are more like a sequence of bursts than a continuous signal. Consequently, for mass ratios relevant to stellar mass BH-NS mergers, the evolution of effective orbital parameters describing the binary is not adiabatic. An interesting coincidence for this class of BH-NS systems is that the range of pericenter separations where the orbit becomes unstable due to general relativistic effects ($r_p \lesssim 10M$ depending upon on the spin of the black hole, where M is the total mass of the system and unless otherwise stated we employ geometric units with $G = c = 1$ throughout) roughly corresponds with the onset of tidal stripping of NS material (depending upon its radius, and hence mass and EOS). Of course, this is also true for quasi-circular inspiral. However, highly eccentric binaries have significantly more angular momentum than quasi-circular binaries at a given separation. This could result in multiple and prolonged episodes of mass transfer and ejected material, and potentially a more massive accretion disk post-merger. That this is happening in the region of unstable orbits implies that the

dynamics of the matter will carry the strongest possible imprint of dynamical, non-linear gravity.

In [9] we presented the first simulations of BH-NS hyperbolic capture and merger for a non-spinning BH and a single equation of state, modeled using general relativistic hydrodynamics (GRHD) (see [13] for an earlier related study using a Newtonian-based hydrodynamics code). We found a striking dependence of the outcome—disk mass, unbound material, GW signal—on the impact parameter. However, astrophysical BHs are expected to form with a range of spins, (see e.g. [25, 26]) and in the quasi-circular case spin was found to be crucial in obtaining significant accretion disks [27–30]. Additionally, there is significant uncertainty about the NS EOS. Since the EOS determines the NS compaction and, hence, the point at which the NS will become tidally disrupted, it will also be an important determinant of the merger outcome. Here, we expand upon the previous analysis and consider initial BH spins aligned and anti-aligned with the orbital angular momentum (with dimensionless spin parameter $a = 0.5$ and $a = -0.5$ respectively), as well as different EOSs (the “2H”, “HB” and “B” models from [31]). Note that there is no *a priori* reason to expect alignment of the BH spin with orbital angular momentum in dynamical capture binaries; this particular choice of spin direction and magnitude was purely motivated as a first, simplest exploration of the effects of spin on the merger. Certainly in future studies a broader expanse of parameters will need to be considered. There is also much room for improvement with the matter description, including more realistic EOSs and additional physics beyond GRHD. For quasi-circular BH-NS inspiral [32], EOS effects were studied in [33–36], the effects of magnetic fields in [37], and higher mass ratio systems (up to 7:1) in [38].

In the remainder of the paper we begin with a brief review of our numerical methods (Sec.II); more details will be given in a companion paper [39]. In Sec. III we describe the particular cases we study. We focus on systems with small initial periapsis, r_p , in part for the practical reason that these binaries merge quickly and are thus computationally tractable, but also because this is the regime where full GR effects will be most strongly manifest, and maximum complementary information to post-Newtonian studies (e.g. [17] or [13]) can be obtained. We present the results of the simulations in Sec. IV. We find that the rich variability in the dynamics and merger outcome as a function of impact parameter is compounded by considering different EOSs and values of BH spin. For example, we find that with prograde spin or a stiffer EOS, significant episodes of mass transfer may occur during non-merger close encounters. Systems where the BH has retrograde spin or that are somewhat less eccentric (than parabolic) can undergo sustained whirling phases before merger that are evident in the GW signal. As in the eccentric binary NS mergers studied in [10], we also find that strong f -mode oscillations in the NS can be excited in close, non-merger encounters (see also an earlier study

of a head-on BH-NS collisions [40]). In Sec. V we use the results of the simulations to calibrate a simple model for the non-adiabatic evolution of effective orbital parameters during each close encounter. This will be used in a future study to build model GW templates and explore the detectability of these systems with gravitational wave observations. We conclude in Sec. VI.

II. NUMERICAL METHODS

In this section, we briefly outline our numerical methods for solving the GRHD equations. More details will be presented in [39], including results from an extensive range of tests.

A. Evolution

We model the evolution of BH-NS binaries by solving the Einstein field equations coupled to a perfect fluid. We solve the field equations in the generalized harmonic form [41–43] with constraint damping [44, 45], where the coordinate degrees of freedom are specified through source functions H^a . We employ fourth order accurate finite difference (FD) techniques and Runge-Kutta time-stepping. In evolving eccentric binaries, we find that a damped harmonic gauge similar to the one described in [46] (see also [47]) is beneficial in achieving stable evolutions through merger.

We describe the neutron star material as a perfect fluid. The fluid equations are written in conservation-law form and solved using high-resolution shock-capturing schemes. Though we have implemented several methods for calculating inter-cell fluxes and for reconstructing fluid primitive variables at cell faces, we used HLL [48] combined with WENO-5 [49] for the results presented here. The fluid is evolved using second order Runge-Kutta time-stepping. To resolve the various length scales, we use Berger and Oliger style adaptive mesh refinement (AMR) [50]. AMR boundaries require special treatment in conservative hydrodynamics codes, since the fluxes emerging from a fine grid region, for example, do not exactly match the incoming flux calculated on the coarse grid (due to their differing truncation errors). To enforce conservation, we correct the adjacent coarse grid cells using the fine grid fluxes, according to the method of Berger and Colella [51]; more details on our particular implementation of this method is given in [39].

Truncation error estimates are used to generate the AMR level structure. All initial data were evolved with a fiducial “medium” resolution run, where the coarsest level has 128^3 cells and covers the entire domain (we use a compactified coordinate system, so this includes spatial infinity), and we chose a maximum truncation error so that initially 6 additional levels of refinement (7 total) are generated to resolve the BH and NS. Given the computational expense of these simulations, we limited the total

number of levels to 7 during evolution, and did not allow regridding on the 2 coarsest levels to prevent the algorithm from tracking the outgoing gravitational waves beyond the largest extraction sphere of $100M$. For several representative cases we also ran a “low” and “high” resolution simulation for convergence testing, where on each level the low (high) resolution run has a mesh spacing of $64/50$ ($64/96$) that of the medium resolution run¹. To give some sense of the smallest scales resolved by the hierarchy, before tidal disruption the low (medium, high) resolution run has two finest level meshes centered around the BH and NS of roughly 80^3 ($100^3, 150^3$) cells each, resolving the diameter of the NS with approximately 40 (50, 75) cells, and the BH horizon diameter with roughly 70 (85, 130) cells. Unless otherwise noted, results will be reported for medium resolution, with error bars (where appropriate) computed from convergence calculations.

B. Initial data

We construct initial data by superimposing a boosted BH with a boosted (non-spinning) TOV star solution separated by $d = 50M$. Though this superposition does not strictly satisfy the constraint equations except in the limit of infinite separation, we have performed tests at various separations in order to verify that the superposition-induced constraint violation is comparable to truncation error at our resolution. In Fig. 1, we show the level of constraint violation ($C_a \equiv H_a - \square x_a$) for various separations and resolutions for the $r_p = 10M$ case. At these resolutions, we can still achieve convergence of the constraints with this superposed data, and increasing the initial separation to $d = 100M$ does not significantly affect the level of constraint violation at the same resolution. This implies that the error introduced by the superposition is on the order of or smaller than the numerical truncation error.

III. CASES

Motivated by possible BH-NS interactions in cores of galactic nuclei and globular clusters, we create initial data for hyperbolic encounters with varying impact parameter. These encounters are hyperbolic since the two bodies have non-zero kinetic energy at (effectively) infinite separation. We will take their relative velocity at infinity to be $w = 1000$ km/s, since this is the expected magnitude of the virial velocity in the core of a nuclear cluster [12, 52].

¹ But note that, except for the 2 coarsest levels, the hierarchies are not identical between the different resolution runs, as it is the local truncation error estimates for each run that guide the construction of the corresponding mesh.

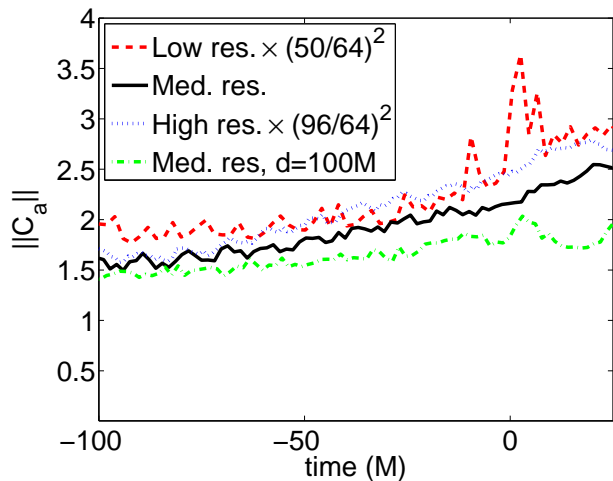


FIG. 1. L^2 -norm of the constraint violation ($C_a \equiv H_a - \square x_a$) in arbitrary units from the $r_p = 10M$ case in the $100M \times 100M$ region around the center of mass in the equatorial plane. This is shown for low, medium, and high resolutions (scaled to the medium resolution assuming second-order convergence) for the standard initial separation between the BH and NS of $d = 50M$. Also shown is a medium resolution run with an initial separation of $d = 100M$. The time is shifted so that the point of closest approach occurs at approximately $t = 0$ for all cases.

In practice, this initially positive total energy is small compared to the kinetic energy of the encounter itself, so that the orbits are nearly parabolic and have eccentricities $1 + O(10^{-5})$. In this study we will also restrict our attention to BH-NS systems with a 4:1 mass ratio.

We choose the initial positions and velocities for the BH and the NS according to the Newtonian equations for a hyperbolic orbit (see, e.g., [53]) with $w = 1000$ km/s and an initial separation of $d = 50M$. We vary the initial spin of the BH, considering the values $a = -0.5, 0$, and 0.5 where negative (positive) values indicate retrograde (prograde) spin in relation to the orbital angular momentum. We also consider three different EOSs: the “2H,” “HB,” and “B” broken Γ -law models from [31]. For the prototypical $1.35 M_\odot$ NS that we use, these give compactness $M_{NS}/R_{NS} = 0.13, 0.17$, and 0.18 respectively. Note that, while the compactness of the B EOS NS is only slightly smaller than that of the HB, it has a maximum mass of $2.0 M_\odot$. Given recent observations [54], B is therefore on the soft end of the allowed range of EOSs. We include a thermal component in the EOS to allow for shock heating.

As mentioned earlier, we do not consider large impact parameters corresponding to initial $r_p > 15M$. Even so, for impact parameters at the upper end of the range we do evolve, the eccentricity is sufficiently large (though < 1) after the first close encounter that it would be prohibitively expensive to evolve to the second encounter. To help calibrate our model for orbital parameter evolu-

tion we introduce in Sec. V, we also consider a set of runs with initial orbital parameters for a bound orbit with eccentricity $e = 0.75$ instead of the hyperbolic orbit with $e \approx 1$. These simulations can be seen as corresponding to systems that have already undergone one or more close encounters, and evolved to these “initial conditions”.

To keep the parameter space at a manageable size, we vary only one of the three parameters of BH spin, NS EOS, and initial eccentricity at a time from our base case — an initially non-spinning BH ($a = 0$), a NS with the HB EOS, and the two objects initially on a marginally unbound orbit ($e \approx 1$) — and then consider a range of impact parameters. See Fig. 2 for plots of the NS trajectory for several cases, and Fig. 3 for snapshots of the rest mass density at select times illustrating aspects of the matter dynamics.

IV. RESULTS

Varying the parameters as discussed in the previous section, there is much degeneracy in the qualitative features that arise (which will need to be addressed in future studies investigating extraction of source properties from GW and EM observations). This is essentially because the leading order source of the variability is rooted in the following two properties of the system: (1) the NS radius, varied by altering the EOS (as the NS mass is fixed in this study), (2) the location of the innermost stable orbit (ISO)², varied by changing the spin of the BH or the eccentricity of the encounter. In terms of the gravitational dynamics, the closer the periapsis is to the ISO, the more whirling that occurs, resulting in enhanced GW emission and more rapid evolution of effective orbital parameters. Regarding the matter dynamics, first, the ISO is essentially the “event horizon” for fluid elements following geodesics, or being close to geodesic. If the periapsis of the orbit is within the ISO, a merger will result. Second, for a 4:1 mass ratio system as studied here, the separation where the NS will begin to overflow its Roche Lobe is close to the ISO. If inside the ISO, the BH-NS system will merge with very little material left post merger. If close to the ISO, the BH-NS system will also merge, though a sizable amount of material could be left, some unbound, some forming an accretion disk. If sufficiently far outside the ISO, material will be stripped from the NS, yet a core of NS material could remain intact moving out to apoapsis before a subsequent encounter; some stripped material will accrete into the

² For equatorial geodesics on a black hole background, these orbits asymptote to circular orbits, though these should not be confused with the innermost *stable* circular orbit (at $r = 6M$ in Schwarzschild), or ISCO. The circular orbits (in the range $r = 3M$ to $6M$ in Schwarzschild) associated with the ISOs with non-zero eccentricity are *unstable*, and under infinitesimal perturbation their non-circular nature is manifest.

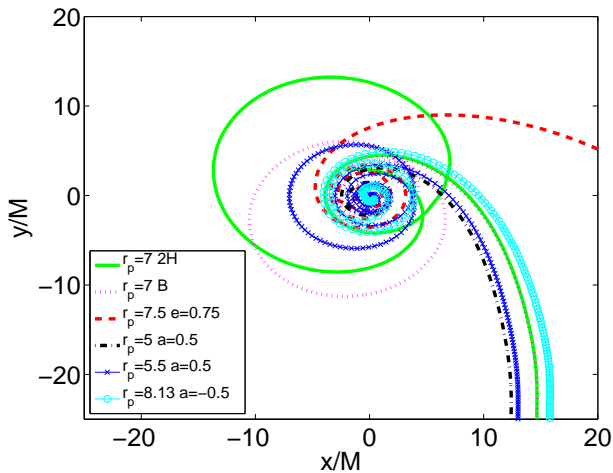


FIG. 2. Trajectories of the NS center of mass for various simulations. The $r_p = 7.0$ with 2H EOS, $r_p = 7.0$ with B EOS, and $r_p = 5.5$ $a = 0.5$ (HB EOS) both undergo a close encounter followed by a short elliptic orbit before merging. Note that while in both the $r_p = 7.0$ cases the NS approaches the BH with the same orbital parameters, the dynamics around the close encounter are very different due to EOS effects (see Sec. IV C). The remainder of the cases shown merge on the first encounter while displaying various degrees of whirling behavior.

BH, some back onto the NS, and a portion will be flung out unbound.

In the following sub-sections, we break down the discussion of phenomenology of the encounters by first summarizing the results from the base case presented in [9] (Sec. IV A), then describe in turn what happens when spin (Sec. IV B), EOS (Sec. IV C) and eccentricity (Sec. IV D) are changed relative to the base case. In order to have some intuitive understanding of why the changes have the effects they do, it is useful to keep the above discussion in mind. This can also allow one to anticipate what would happen if parameters we are not altering here are changed, for example the BH or NS mass.

A. Zero-spin survey with HB EOS

Here we summarize the results obtained for simulations with an initially non-spinning BH and a NS with the HB EOS (see [9] for more details). We considered a range of periapsis separations from $r_p/M = 5.0$ to 15 (*i.e.*, 50 to 150 km). (Henceforth, we will consider r_p to be normalized by M .) In all of these cases, sufficient energy is carried away by GWs to result in a bound system. Our simulations exhibit three types of behavior: (1) a direct plunge ($r_p = 5.0, 5.83, 6.67, 6.81$), (2) following the initial periapsis passage, a single elliptical orbit and then a plunge ($r_p = 6.95, 7.22, 7.5$), and (3) following the initial periapsis passage, a long-period elliptical orbit ($r_p = 8.75, 10.0, 12.5, 15.0$). For the latter group

(and the high resolution $r_p = 7.5$ run), the entire orbit is prohibitively long to simulate, and we focus on the burst of GWs associated with the first periapsis passage. For one case in each class ($r_p = 5.0, 7.5, 10.0$) we performed a convergence study. The GW energy and angular momentum emitted as well as the disk properties of those cases followed through merger are summarized in Table I. Table II shows the spin of the post-merger BH (for this base set of runs as well as the subsequent parameter survey) for the cases we followed through merger. As the threshold in r_p dividing (1) and (2) is approached there is a dramatic enhancement in the gravitational energy and angular momentum released during the close encounter.

The amount of material remaining after merger which could potentially form an sGRB-powering accretion disk also depends significantly on impact parameter. Below the threshold dividing (1) and (2), there is a sizable amount of remaining material, in excess of 20% in the $r_p = 6.81$ case. In most cases $\approx 50\%$ of the material is unbound. A simple numerical estimate of the fallback time for the bound material based on when the elliptical orbit will return to the accretion disk shows the characteristic $t^{-5/3}$ scaling [55].

B. Effects of black hole spin

As expected from Kerr geodesics, prograde BH spin results in a smaller impact parameter below which the NS merges with the BH on the first encounter than in the non-spinning case. Conversely, for the cases with retrograde initial BH spin, the critical impact parameter is larger. For the cases with initial BH spin $a = 0.5$ (top of Table III), only the $r_p = 5.0$ case merges on the first encounter while those with $r_p = 5.5, 6.0$, and 6.25 go back out on a short elliptic orbit before merging. The $r_p = 7.5$ and 10.0 cases go out on a long elliptic orbit after the initial periapsis passage, and we did not follow these through merger. For the $r_p = 5$ case, we also performed convergence tests in order to estimate truncation error for a spinning BH where the effective ISO is closer to the BH. One important consequence of the reduced critical impact parameter in the prograde case is that, around this threshold, the tidal forces on the NS are greater and the resulting accretion disks consequently larger. Even more striking, the enhanced tidal interaction can lead to significant mass transfer from the NS to the BH even in non-merger close encounters, as for example with the $r_p = 5.5, a = 0.5$ case. Here the NS becomes highly distorted and loses approximately 16% of its mass to the BH (see Fig. 4). However, a compact (albeit highly distorted) star remains (see Fig. 3 middle, bottom) until it merges with the BH on its second close encounter.

For the $a = -0.5$ cases (bottom of Table III), $r_p = 5.0, 7.5$, and 8.13 were direct mergers, while the $r_p = 8.28$ case goes through a single elliptic orbit before merging. The $r_p = 8.44, 8.75$, and 10.0 cases go out on longer elliptical orbits which we did not follow to completion. Because

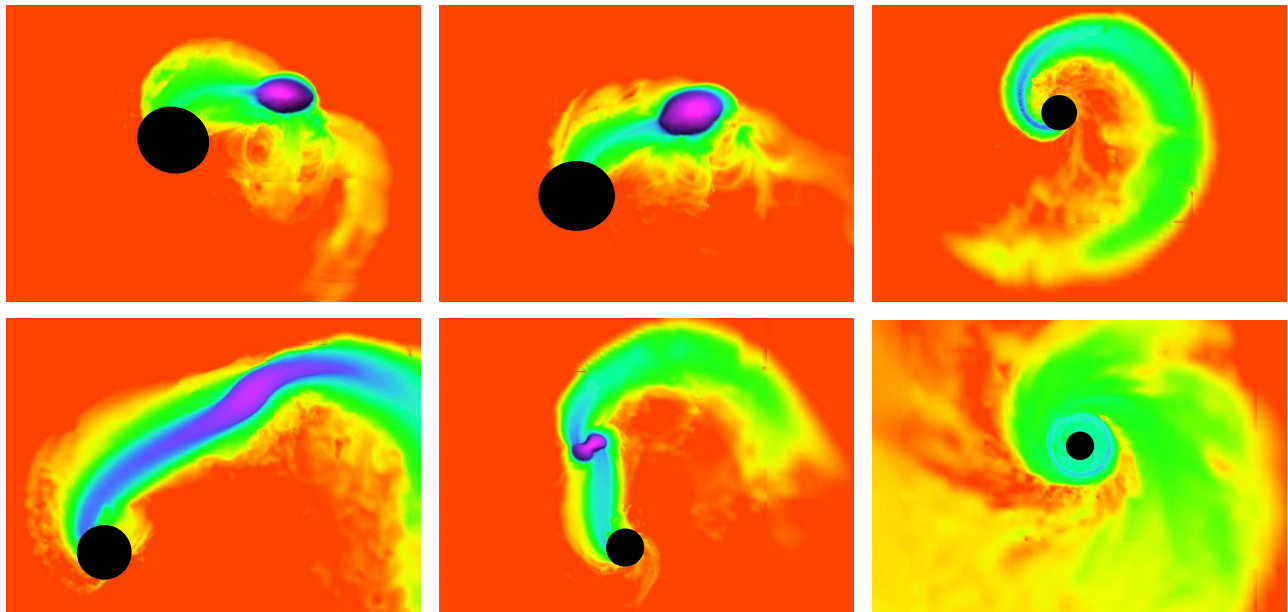


FIG. 3. Rest mass density in the equatorial plane from various BH-NS simulations, left to right, top to bottom: (1) the BH and NS undergoing a close-encounter ($t = 242 M$, $r_p = 7.0$, B EOS), (2) the NS undergoing a whirling phase before merging ($t = 269 M$, $r_p = 8.13$ $a = -0.5$), (3) the NS stretched into a long tidal stream during merger ($t = 506 M$, $r_p = 7.5$ $e = 0.75$), (4) a mass transfer episode ($t = 292 M$, $r_p = 7.0$, 2H EOS), (5) towards the end of a mass transfer episode during the NS's first periapsis passage ($t = 272 M$, $r_p = 5.5$ $a = 0.5$), and (6) a nascent accretion disk ($t = 388 M$, $r_p = 5$ $a = 0.5$). Recall that r_p is reported in units of The color scale is logarithmic from 10^{-6} to 1 times the initial maximum density ($\rho_{\max} = 8.3$ (3.7,9.8) $\times 10^{14}$ g cm $^{-3}$ for the HB (2H, B) EOS). The BH is roughly the same coordinate size in all panels, which can be used to infer the relative scale of each snapshot. total mass M .

r_p	$M_0/M_0(t=0)^a$	$M_{0,u}/M_0(t=0)^b$	τ_{acc} (ms) ^c	First periapsis ^d		Total ^e	
				$\frac{E_{\text{GW}}}{M} \cdot 10^2$	$\frac{J_{\text{GW}}}{M^2} \cdot 10^2$	$\frac{E_{\text{GW}}}{M} \cdot 10^2$	$\frac{J_{\text{GW}}}{M^2} \cdot 10^2$
5.00	0.005	0.0	25	–	–	0.67(0.87) ^f	4.14(4.86) ^f
6.67	0.107	0.056	130	–	–	1.29	9.10
6.81	0.221	0.101	40	–	–	1.19	9.60
6.95	0.018	0.003	47	0.697	7.33	1.65	13.9
7.22	0.013	0.001	16	0.358	4.48	1.18	10.2
7.50	0.009	0.003	7.6	0.242(0.147) ^f	3.44(2.46) ^f	1.03	44.7
8.75	0.073	1.58
10.0	0.033(0.027) ^f	0.97(0.88) ^f
12.5	0.011	0.46

TABLE I. Disk properties and GW energy and angular momentum losses for an initially hyperbolic ($e \approx 1$) encounter of a zero spin BH and NS with HB EOS. Dashed entries correspond to cases that merge during the first encounter, and hence have no “first periapsis”; dotted entries correspond to binaries that were only evolved through first periapsis passage.

^a Rest mass remaining outside the BH shortly after merger, normalized by the initial total rest mass.

^b Unbound rest mass estimated using local fluid velocities.

^c Rough *initial* accretion timescale ($\tau_{\text{acc}} = M_0/\dot{M}_0$) evaluated shortly after merger.

^d Energy and angular momentum lost to GWs during the first close encounter.

^e Total GW energy and angular momentum losses for cases which were followed through merger.

^f Results are from medium resolution runs; values in parentheses are Richardson extrapolated estimates using low and high resolutions, where available. Note that the relatively large error for $r_p = 7.5$ (and to a lesser extent $r_p = 5, 10$) is due in part to truncation error altering the actual periapsis by a small amount, and in this regime the GW emission is highly sensitive to binary separation (Figure 10).

$a = 0$ HB EOS								
r_p	5.00	6.67	6.81	6.95	7.22	7.50		
a_{final}	0.49 ^a	0.45	0.37	0.47	0.50	0.50		
a_{eff}	0.40	0.46	0.47	0.47	0.48	0.49		
$a = 0.5$			$a = -0.5$					
r_p	5.00	5.50	6.00	6.25	5.00	7.50	8.13	8.28
a_{final}	0.74	0.71	0.71	0.70	0.16	0.25	0.22	0.24
a_{eff}	0.72	0.74	0.77	0.77	0.08	0.17	0.19	0.19
2H EOS				B EOS				
r_p	5.00	6.75	7.00		5.00	6.25	7.00	
a_{final}	0.50	0.29	0.33		0.48	0.52	0.48	
a_{eff}	0.40	0.46	0.47		0.40	0.45	0.47	
$e = 0.75$								
r_p	7.50	7.81						
a_{final}	0.44	0.49						
a_{eff}	0.46	0.47						

^a $a_{\text{final}} = 0.49 \pm 0.01$

TABLE II. Post-merger BH spin (dimensionless) for various initial conditions. Also shown is the effective spin, a_{eff} , used in the model described in Sec. V and calculated from initial conditions using (2).

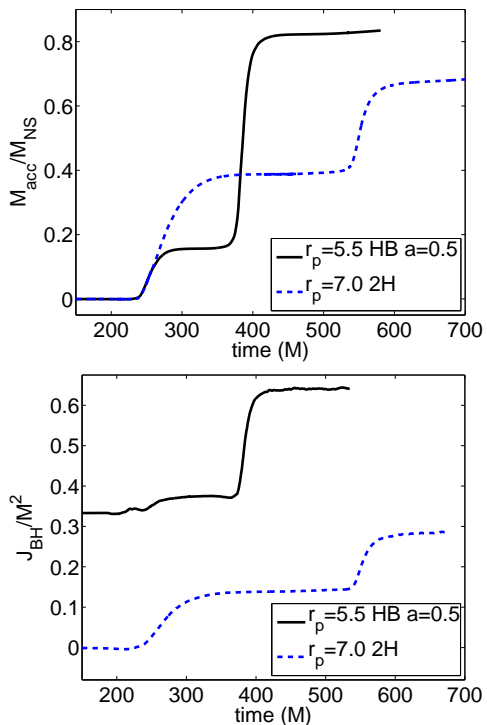


FIG. 4. **Top:** The amount of rest mass (normalized to the total rest mass of the NS) accreted by the BH as a function of time for the $r_p = 7.0$ 2H case and for the $r_p = 5.5$, $a = 0.5$ HB case. In both cases there are two significant episodes of mass transfer. **Bottom:** The angular momentum of the BH horizon as a function of time for the same two cases.

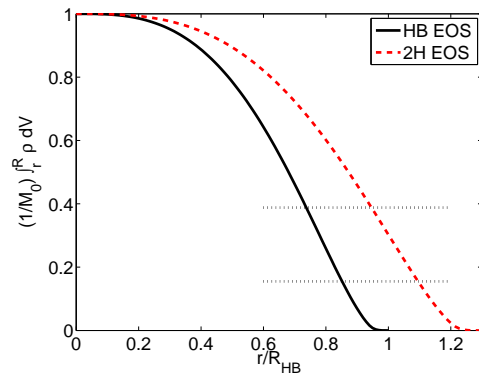


FIG. 5. The fraction of rest mass outside a given radius, $(1/M_0) \int_r^R \rho dV$, for an isolated star with the HB or 2H EOS and $M = 1.35 M_\odot$. Here radius, r , is normalized to the radius of the HB star (R_{HB}). The horizontal, dotted lines indicate the amount of material accreted into the BH during the initial close encounter for the $r_p = 5.5$ case with HB EOS (bottom) and the $r_p = 7.0$ case with 2H EOS (top) as shown in Fig. 4.

of the larger critical impact parameter for merger on the first encounter, there is less tidal disruption and hence the accretion disks contain $\leq 1\%$ of the total NS rest mass for all the cases followed through merger. However this also means that the BH and NS can undergo more whirling behavior in the critical regime before merger. This is especially evident in the waveform for the nearer threshold merger case of $r_p = 8.13$, $a = -0.5$ as shown in Fig. 8. The gravitational wave signal shows several cycles of almost constant amplitude and phase, indicative of a nearly circular orbit. Compared to the near threshold non-spinning case ($r_p = 6.81$, also shown in Fig. 8), this whirling period is much more pronounced in the waveform.

C. Effects of equation of state

We also considered two additional EOSs: the B which is softer than the HB and the 2H which is stiffer. Though the different EOSs have only a slight effect on the critical impact parameter, they can have a dramatic effect on the near-threshold behavior. For the B EOS, we chose four different impact parameters (bottom of Table IV): $r_p = 5.0$ and 6.25 (direct mergers); $r_p = 7.0$ (after periapsis passage, a short elliptic orbit and then merger); and $r_p = 7.5$ which we did not follow through its full elliptic orbit after the first close encounter. The more compact B EOS NS experiences less tidal disruption and forms accretion disks with $\leq 1\%$ of the total NS rest mass for all cases followed through merger. For the 2H EOS, we considered five different impact parameters (top of Table IV): $r_p = 5.0$ and 6.75 (direct mergers); $r_p = 7.0$ (after periapsis passage, a short elliptic orbit and then merger); and $r_p = 7.25$ and 7.5 which we did not follow through the full

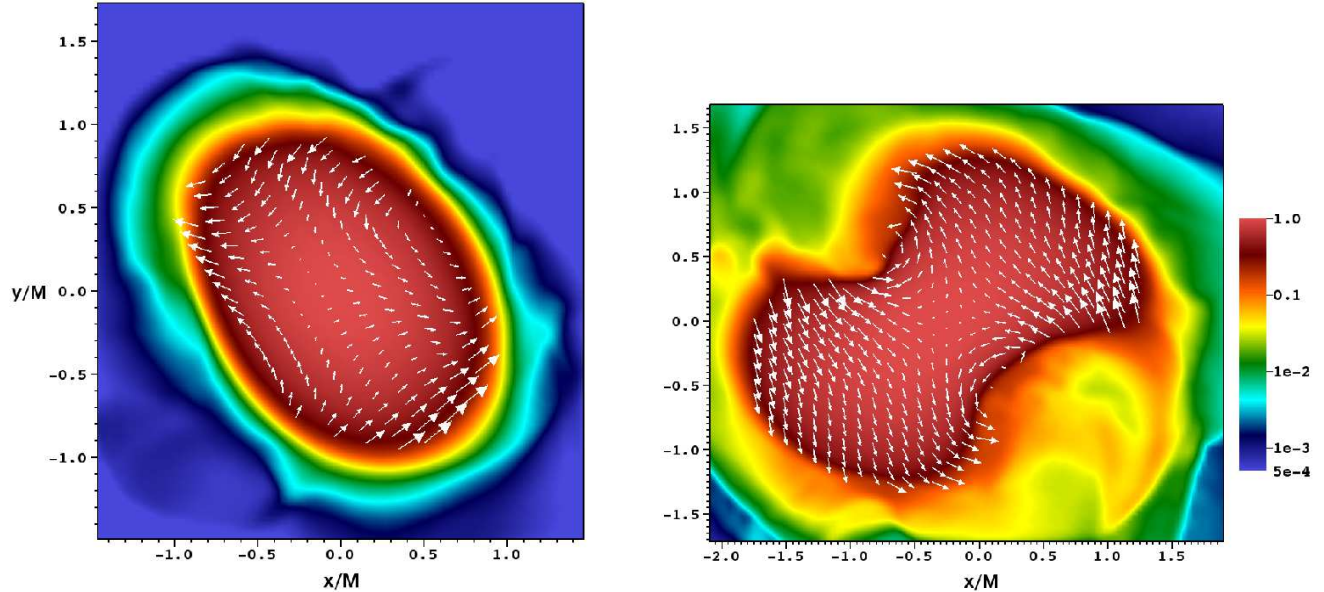


FIG. 6. NSs exhibiting large-amplitude f -mode oscillations following the first interaction with the (non-spinning) BH. The cases shown are $r_p = 6.95$ with the HB EOS at $t = 341M$ (left) and $r_p = 7.0$ with the 2H EOS at $t = 356M$ (for the latter case see the bottom left panel of Fig. 3 for a snapshot of the density near the time of closest approach to the BH when this large oscillation is excited). The color map shows the rest-mass density in the equatorial plane on a logarithmic scale, normalized to the instantaneous maximum density. The arrows show the velocity in the NS center of mass frame. The longest velocity arrows correspond to velocity magnitudes 0.084 (left) and 0.17 (right). Though the two cases have similar periapsis radii, the lower compaction in the 2H case leads to a much stronger tidal interaction and an f -mode which shows non-linear characteristics.

r_p	$M_0/M_0(t=0)^a$	$M_{0,u}/M_0(t=0)^b$	τ_{acc} (ms) ^c	First periapsis ^d		Total ^e	
				$\frac{E_{\text{GW}}}{M} \cdot 10^2$	$\frac{J_{\text{GW}}}{M^2} \cdot 10^2$	$\frac{E_{\text{GW}}}{M} \cdot 10^2$	$\frac{J_{\text{GW}}}{M^2} \cdot 10^2$
$a = +0.5$							
5.00	0.139	0.021	4.8	–	–	1.25(1.41) ^f	7.14(9.04) ^f
5.50	0.174	0.088	40	0.800	7.14	1.40	10.9
6.00	0.181	0.029	26	0.360	4.16	1.53	14.7
6.25	0.080	0.014	33	0.347	4.11	1.29	12.0
7.50	0.104	1.90
10.0	0.025	0.82
$a = -0.5$							
5.00	0.007	0.0	36	–	–	0.33	2.32
7.50	0.008	0.0	71	–	–	0.82	5.91
8.13	0.010	0.0	0.12	–	–	1.57	13.7
8.28	0.002	0.0	2.8	0.385	5.12	1.25	12.8
8.44	0.268	3.98
8.75	0.167	2.85
10.0	0.052	1.32

TABLE III. Disk properties and GW energy and angular momentum losses for an initially hyperbolic ($e \approx 1$) encounter of a BH with spin $a = \pm 0.5$ and NS with HB EOS. The same comments and set of footnotes ^a to ^f apply as in Table I.

elliptic orbit after the first close encounter.

The less compact 2H EOS NS experiences significant tidal deformation, and for the $r_p = 6.75$ and 7.0 cases there is $\approx 30\%$ of the NS material leftover post-merger. In the case of $r_p = 7.0$ the deformation and tidally-induced oscillations of the NS are especially severe (see Fig. 3, bottom left) and there is a period of significant mass transfer (Fig. 4) from the NS to the BH during the first close encounter. This is very similar to the $r_p = 5.5, a = 0.5$ case, though more pronounced. Since with both the 2H EOS and the $a = 0.5$ with HB EOS simulations no significant mass transfer is found for runs with r_p slightly above 7.0 and 5.5 respectively, we can use these as an effective measure of the separation d_R at which the star begins to overflow its Roche lobe. Though the individual values are somewhat higher than expected from Newtonian theory, it predicts a scaling with compaction $d_R \propto C_{NS}^{-1}$ where $C_{NS} \equiv M_{NS}/R_{NS}$, that does approximately hold here since $C_{HB}/C_{2H} = 1.3$. This of course ignores any relativistic effects, both gauge and physical, the latter including for example the effect of BH spin on tidal disruption. In Fig. 5 we show the mass profiles of an isolated star with the 2H and HB EOS. This shows that the outer spherical shell which contains approximately 40% of the material accreted into the BH during the first close encounter for 2H corresponds to a volume containing almost no material in the HB case. Again, though we are ignoring the complicated details of mass transfer dynamics, this is suggestive as to why, for the BH-NS system studied here, there is significant mass transfer for the 2H EOS around $r_p = 7.0$ but very little for the HB EOS.

Since for the 2H, $r_p = 7.0$ case so much mass is transferred before the merger and there is a strong disruption during merger, the gravitational wave signal resulting from merger itself is significantly weaker than other cases (see Fig. 8). The full waveform from this case (Fig. 9) also shows that the GW pulse from the fly-by dominates the signal compared to the merger part of the waveform.

In between the initial close encounter and merger there is also evidence in the GW signal of excited f -modes within the NS; this was also observed in eccentric binary NS encounters [10]. Here we give a qualitative account of the stellar dynamics to show that the dominant oscillation is akin to that of an f -mode of an isolated, perturbed star—a detailed study, aside from the difficulty of applying a perturbative analysis in such a transient and in some cases highly distorted star, is beyond the scope of this study. Fig. 6 demonstrates the density and velocity distortions for the $r_p = 7.0$, 2H case (right panel) as well as the $r_p = 6.95$, HB case, in which the distortion is less extreme (left panel). The latter bears a particularly strong resemblance to the pure $l = m = 2$ f -mode flow pattern (see, *e.g.*, Fig. 19 of [56]). In both cases, an animation of the density field seems to suggest a rotating, distorted NS. However, as Fig. 6 demonstrates, the velocity pattern is not one of overall rotation, but rather that of an oscillatory mode. Indeed,

the circulation theorem should hold to a good approximation in the bulk of the NS material (though there are entropy-generating shocks near the surface). Thus, the tidal interaction with the BH would not induce rotation in the usual sense, but rather oscillatory modes with rotating patterns. Many such modes are likely to be excited, but the $l = m = 2$ f -mode seems to dominate. We performed a spherical-harmonic decomposition of the star’s rest mass density, $\rho = \sum C_{lm} Y_{lm}$, at select times and found C_{22} to be the largest coefficient next to C_{00} . We also checked that the perturbation amplitude grows monotonically with radius. For the $r_p = 6.95$ simulation with the HB EOS, $|C_{22}/C_{00}| \approx 0.01 - 0.02$ at $r = 0.4M$ and grows to $|C_{22}/C_{00}| \approx 0.15 - 0.20$ at $r = 0.8M$. The next largest coefficient, C_{20} , is smaller by a factor of $\gtrsim 2$. The $r_p = 7.0$ simulation with the 2H EOS shows similar behavior though the coefficients are somewhat larger with $|C_{22}/C_{00}| \approx 0.03$ and 0.25 at $r = 0.4M$ and $0.8M$ respectively.

D. Bound eccentric evolution

Finally, we simulated binaries where the BH and NS have initial orbital parameters corresponding to a bound orbit with $e = 0.75$ for a range of values of r_p . These simulations can be viewed as corresponding to systems that have already become bound through one or more close encounters and lost some of their initial eccentricity. In practice, such evolutions would be prohibitively long to follow in full. Of the impact parameters considered (see Table V), $r_p = 7.5$ is the only direct plunge, and $r_p = 7.81$ is the only case we followed past periastris passage to merge on the second close encounter. The remaining cases ($r_p = 8.13, 8.75,$ and 10.0) we only followed partially through their elliptic orbits after the first close encounter. The threshold for merger on the first encounter moves out slightly in this case as an appeal to geodesics in Schwarzschild would suggest. In Fig. 7, we plot the gravitational waveforms from two fly-by close encounters, $r_p = 8.13$ and 10.0 . In addition we fit the expected waveform according to a Newtonian-order quadrupole approximation [53, 57] (NQA) to our numerical results by multiplying by an overall factor. As found in [9] and in our other simulations here for the marginally unbound case, though the shape of the waveforms agree quite well, the numerical results exhibit a significant amplitude enhancement that is larger the closer one gets to the threshold for merger during the close encounter. In addition, from Fig. 8 we can see that the near-threshold merger waveform shows more evidence of whirling than the initially unbound case.

V. EVOLUTION OF ORBITAL PARAMETERS

As noted in [9], there is a dramatic enhancement in gravitational wave energy and angular momentum emit-

r_p	$M_0/M_0(t=0)^a$	$M_{0,u}/M_0(t=0)^b$	τ_{acc} (ms) ^c	First periapsis ^d		Total ^e	
				$\frac{E_{\text{GW}}}{M} \cdot 10^2$	$\frac{J_{\text{GW}}}{M^2} \cdot 10^2$	$\frac{E_{\text{GW}}}{M} \cdot 10^2$	$\frac{J_{\text{GW}}}{M^2} \cdot 10^2$
2H EOS							
5.00	0.008	0.0	56	–	–	0.58	3.61
6.75	0.278	0.117	18	–	–	0.47	4.65
7.00	0.303	0.149	60	0.387	4.53	0.43	5.41
7.25	0.283	3.90
7.50	0.200	3.07
B EOS							
5.00	0.008	0.0	57	–	–	0.60	3.83
6.25	0.008	0.0	64	–	–	0.87	5.63
7.00	0.010	0.001	10	0.718	7.69	1.73	10.7
7.50	0.268	3.72

TABLE IV. Disk properties and GW energy and angular momentum losses for an initially hyperbolic ($e \approx 1$) encounter of a BH with zero spin and a NS with 2H and B EOS. The same comments and set of footnotes ^a to ^f apply as in Table I.

r_p	$M_0/M_0(t=0)^a$	$M_{0,u}/M_0(t=0)^b$	τ_{acc} (ms) ^c	First periapsis ^d		Total ^e	
				$\frac{E_{\text{GW}}}{M} \cdot 10^2$	$\frac{J_{\text{GW}}}{M^2} \cdot 10^2$	$\frac{E_{\text{GW}}}{M} \cdot 10^2$	$\frac{J_{\text{GW}}}{M^2} \cdot 10^2$
7.50	0.109	0.062	32	–	–	1.47	13.6
7.81	0.007	0.001	7.1	0.410	5.25	1.58	16.1
8.13	0.248	3.67
8.75	0.125	2.34
10.0	0.049	1.28

TABLE V. Disk properties and GW energy and angular momentum losses for an initially eccentric $e = 0.75$ encounter of a zero spin BH with a NS with HB EOS. The same comments and set of footnotes ^a to ^f apply as in Table I.

ted in a BH-NS close encounter that occurs as the threshold for merger on the first encounter is approached. In this section, we will attempt to explain this enhancement by analogy to the zoom-whirl orbits in Kerr spacetimes and extrapolate this behavior to close encounters with different eccentricities and spins. Then we will use these results to approximate the evolution of orbital parameters for BH-NS systems undergoing a series of close encounters.

A. Zoom-whirl enhancement

As discussed in the previous section and as can be seen in Fig. 10, though different values of initial spin or eccentricity may shift the critical value of r_p , which we shall call r_c , at which the NS merges with the BH during a first encounter, for all the cases considered there is a significant enhancement in the energy of the gravitational waves emitted as this threshold is approached. This can be understood by analogy to the zoom-whirl orbits in Kerr spacetimes. As the BH-NS approaches the critical impact parameter, it is closer and closer to the unstable orbit dividing plunging and non-plunging orbits and will therefore exhibit more and more whirling behavior.

Though the effect is most dramatic near threshold, this zoom-whirl analog is a way to understand the significant enhancements over the NQA predictions that persist till $r_p \approx 10$ (see Fig.4 in [9]). This motivates a fit to the GW energy emitted in a whirling close encounter with the functional form (see Fig. 10)

$$E_{\text{GW}} = E_0(1 - (\delta r_p/\Delta)^\gamma) \quad (1)$$

where $\delta r_p = r_p - r_c$, E_0 is the difference in energy between a quasi-circular orbit and an eccentricity e orbit both with $r_p = r_c$, Δ is the range over which zoom-whirl like behavior dominates the GW emission energetics (we take $\Delta = 3$), and γ is a parameter that in the geodesic analogue is related to the instability exponent of the corresponding unstable circular orbit; here, we use it as our fitting parameter. The top panel of Fig. 10 shows this fitting performed individually to each set (e, a) of simulations run. In the remainder of this section we will use the data from the $e \approx 1$, $a = 0$ set to calibrate geodesic-inspired extensions to arbitrary values of (e, a) , which can then be compared to the other 3 sets of simulation data (bottom panel of Fig. 10) to test how well this extrapolation works.

To extend this model to different values of eccentricity e and BH spin a , we assume that the dependency of r_c

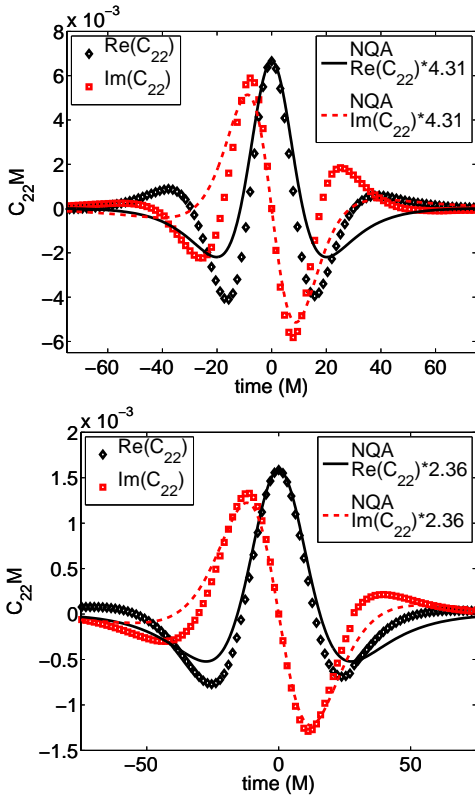


FIG. 7. The real and imaginary components (black diamonds and red squares) of the $l = 2$, $m = 2$ spherical harmonic of $r\Psi_4$ for $e = 0.75$ and $r_p = 8.125$ (left) and $r_p = 10$ (right). For comparison the NQA analytical results are shown multiplied by an overall factor so that the magnitude and phase match at peak ($t = 0$).

and γ on these values is the same as in the geodesic case on a Kerr background. We will use a_{eff} to refer to the effective spin parameter we use in the Kerr formulae. For better correspondence with the Kerr spacetime we want to take a_{eff} to be the approximate spin of the BH that would form if a merger occurred. We estimate a_{eff} using

$$a_{\text{eff}} = a_0 \frac{\sqrt{(1+e)r_p}}{\sqrt{2r_{c0}}} + a(M_{\text{BH}}/M)^2. \quad (2)$$

where M_{BH} , a , r_p , and e are the initial BH mass, initial BH spin, periapsis and eccentricity respectively of the encounter we want to compute an a_{eff} for, and $a_0 \approx 0.5$ is the final spin measured from the $e \approx 1$, $a = 0$, $r_p = r_{c0} \approx 6.9$ simulation. In Table II we show how a_{eff} compares to the final BH spins in the simulations that we followed through merger. Though this simple formula based on the total angular momentum of the system does not attempt to capture any of the complications due to differences in matter dynamics or gravitational radiation between the different cases, it does a decent job of estimating the final BH spin for the purposes of this model.

Recall that for equatorial geodesics with eccentricity e in Boyer-Lindquist coordinates with BH spin parameter

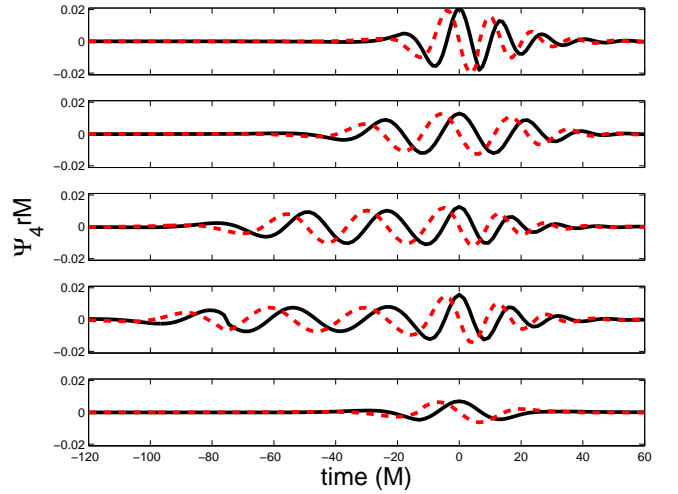


FIG. 8. The real and imaginary components (solid black lines and red dotted lines) of Ψ_4 on the z -axis (perpendicular to the orbital plane) during merger for the following cases (top to bottom): $r_p = 5$ HB, $r_p = 6.81$ HB, $r_p = 7.5$, $e = 0.75$ HB, $r_p = 8.13$, $a = -0.5$ HB, and $r_p = 7.0$ 2H (see Fig. 9 for the full signal). The waveforms are aligned so that the peak occurs at $t = 0$ with zero phase.

a , there is a value for the periapsis which corresponds to a marginally unstable orbit, $r_c^{\text{BL}}(e, a)$. It can be found by solving the equation (see for example [58]) $(r_c^{\text{BL}})^2 = (J - aE)^2(1 + e)/(3 - e)$ where E and J are the orbit's specific energy and angular momentum, respectively. For our model, we assume that $r_c(e, a_{\text{eff}}) \propto r_c^{\text{BL}}(e, a_{\text{eff}})$ and we fit the proportionality constant using our numerical results for $e \approx 1$, $a = 0$.

The instability exponent for unstable circular orbits in Boyer-Lindquist coordinates is given by [59, 60]

$$\gamma^{\text{BL}}(e, a) = \frac{r}{2\pi} \left[3r^2\Delta + \frac{4M}{\omega^2}(rR^2\omega^2 - 4Ma\omega - r + 2m) \right]^{-1/2} \quad (3)$$

where $R = r^2 + a^2(1 + 2M/r)$, $\Delta = r^2 + a^2 - 2Mr$, $\omega = M/(Ma \pm \sqrt{Mr^3})$ (\pm for prograde and retrograde respectively), and we set $r = r_c^{\text{BL}}(e, a)$. Again we assume that $\gamma(e, a_{\text{eff}}) \propto \gamma^{\text{BL}}(e, a_{\text{eff}})$ and fit the proportionality constant using our numerical results for $e \approx 1$, $a = 0$. For the angular momentum lost to gravitational waves in a close encounter we assume a similar expression

$$J_{\text{GW}} = J_0(1 - (\delta r_p/\Delta)^\gamma) \quad (4)$$

where again J_0 is the angular momentum of a quasi-circular orbit evaluated at the same separation r_p .

This simple prescription for estimating gravitational wave energy and angular momentum loss has some obvious limitations. We are extrapolating the critical impact parameter and instability exponent based on a Kerr spacetime to a BH-NS spacetime that is dynamic and

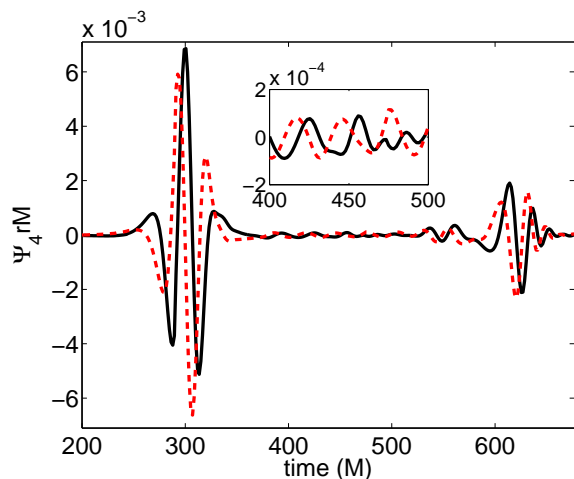


FIG. 9. The real and imaginary components (solid black lines and red dotted lines) of Ψ_4 on the z -axis (perpendicular to the orbital plane) at $r = 70$ M for the $r_p = 7.0$ 2H simulation. The large burst at $t \approx 300$ M comes from the initial fly-by where the NS becomes extremely distorted (Fig. 3) and loses a significant portion of its mass (Fig. 4). The smaller pulse at $t = 600$ M comes from the merger. In between, there is a smaller component of the signal coming from the tidally-induced oscillation of the NS.

non-perturbative. We are also ignoring tidal effects or dependence on EOS in this model. Nevertheless, in Fig. 10, we compare how closely this predicted scaling with spin and eccentricity matches that from simulation results. Given its simplicity, as well as the numerical error in the simulations results, this model does a satisfactory job of capturing the trends in these scalings.

B. Systems undergoing multiple close encounters

The enhanced GW energy and angular momentum losses during a close encounter for a given r_p result in more rapid loss of eccentricity and larger rate of decrease of r_p of the next encounter. Fig. 11 shows approximate trajectories in e and r_p for binaries on initially marginally unbound (*i.e.* $e = 1 + \epsilon$) orbits for a range of initial BH spin. These results were obtained using the above model for energy and angular momentum lost to GWs. We approximate these losses as occurring in discrete steps during close encounters. (This approximation will break down as $e \rightarrow 0$.) Trajectories computed with the Newtonian amplitude and eccentricity dependence are also shown [53, 57, 61]. The Newtonian trajectories execute many more orbits before merger. This clear departure from the Newtonian prediction at small r_p due to strong field GR effects should thus be apparent in the gravitational waveform. This model can also be used to predict approximately the critical initial impact parameter for the BH-NS system to merge on the second close en-

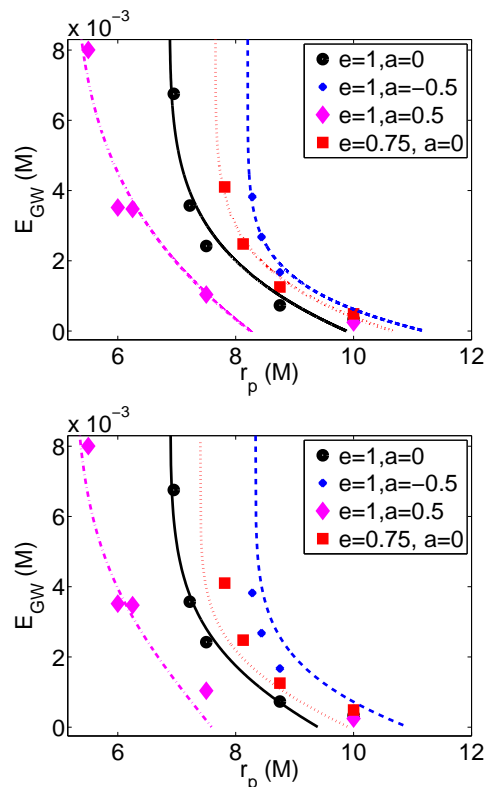


FIG. 10. **Top:** Energy lost to GWs during the initial close encounter (*i.e.* excluding merger) as a function of r_p for initial BH spin $a = 0, -0.5$, and 0.5 and for initial eccentricity $e = 1$ and 0.75 . The functional form $E_0(1 - (\delta r_p/\Delta)^\gamma)$ (lines), motivated by zoom-whirl dynamics, is a fit to the simulation results (points). $\delta r_p = r_p - r_c$, with r_c the threshold value for merger during the encounter. E_0 is the difference in energy between a quasi-circular orbit and an $e \approx 1$ (0.75) orbit, both having $r_p = r_c$. Δ is the range over which zoom-whirl like behavior dominates the GW emission energetics. γ is a parameter that in the geodesic analogue is related to the instability exponent of the corresponding unstable circular orbit; here, we use it as our fitting parameter. We obtain $\gamma = 0.19, 0.13, 0.25$, and 0.16 for $(e, a) = (1, 0), (1, -0.5), (1, 0.5)$, and $(0.75, 0)$ respectively. **Bottom:** This shows the same simulation data points as the top figure, though here we only directly fit (solid black line) to the $e = 1, a = 0$ case (solid black points), and use the method described in the text to extrapolate the values of r_c and γ to the other three cases.

counter, the third close encounter, and so on. We expect interesting dynamics around each of the thresholds up until the point where the system has undergone enough close encounters that it circularizes.

VI. CONCLUSION

We have performed an initial survey of eccentric BH-NS mergers including the effects of black hole spin and varying the NS EOS. Though the limited number of val-

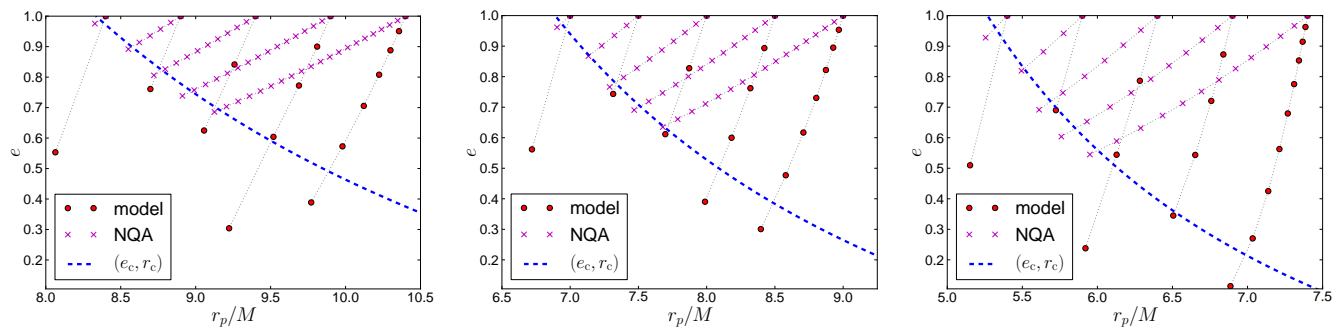


FIG. 11. The evolution of the eccentricity and periapsis separation of various 4 : 1 mass ratio BH-NS binaries that begin marginally unbound and undergo a series of close encounters (large red points) before merging. For comparison, we also plot the results using the Newtonian order expressions from [53, 61] (magenta x’s). We also plot the critical eccentricity for a given r_p for a close encounter to result in merger (dotted blue line). Hence the points below this curve correspond to merger events. From left to right the plots correspond to an initial BH spin of $a = -0.5, 0$, and 0.5 respectively.

ues we considered in this work does not begin to exhaust the parameter space, what is immediately apparent is the strong diversity in the resulting gravitational and matter dynamics. Though we have not yet studied the consequences of this on gravitational wave detectability and parameter extraction, nor possible electromagnetic counterparts, it is clear that the outcome can depend sensitively on the binary parameters and matter EOS. Whether dynamical capture BH-NS mergers occur with sufficient frequency in the universe to constitute a decent event rate for ground-based GW detectors is another question; at the least, failure to observe such events will place constraints on these sources, while if several are observed, given the sensitivity of the outcome to properties of the binary, they could be ideal environments to reveal the structure of neutron stars. And again, we should emphasize that excessive fine tuning of parameters is not required for significant variability. Taking the relative velocity at large separations in a typical nuclear cluster cusp as an example (≈ 1000 km/s), roughly 30% of such encounters will have $r_p \lesssim 10$, corresponding to the cases studied here. Certainly some of the most extreme examples of mass transfer, large accretion disks or multiple whirl orbits will be rare; perusing Tables I-V will give some idea of the distribution with r_p . (Note that the cross section scales linearly with r_p due to gravitational focusing, and that one would also expect some cases with larger initial r_p than we followed through merger to exhibit similar variability.) It is not trivial to calculate a transition value of initial r_p above which the qualitative behavior at late times is described by a quasi-circular inspiral, though our study suggests at *least* a quarter of

dynamical capture binaries will merge with high eccentricity.

For future work, we plan to investigate the detectability of the GW signals from BH-NS mergers that arise from dynamical capture in the strong field regime. This will complement the first study of such systems presented in [17], in that we intend to focus on the latter stages of high eccentricity mergers, including the merger/ringdown part of the signal. Future work also includes expanding the parameter space to different BH and NS masses, BH spin orientations, and (as computational resources permit) evolution of systems that exhibit more than two close encounters before merger. It would also certainly be interesting to investigate EM counterparts to these events; such simulations would require extensions to the code used here beyond the present GRHD.

ACKNOWLEDGMENTS

We thank Adam Burrows, John Friedmann, Roman Gold, Janna Levin, Charalampos Markakis, Benjamin Lackey, Sean McWilliams and Richard O’Shaughnessy for useful conversations. This research was supported by the NSF through TeraGrid resources provided by NICS under grant TG-PHY100053, the Bradley Program fellowship (BCS), the NSF Graduate Research Fellowship under grant DGE-0646086 (WE), NSF grants PHY-0745779 (FP) and PHY-1001515 (BCS), and the Alfred P. Sloan Foundation (FP). Simulations were also run on the **Woodhen** cluster at Princeton University.

[1] A. Abramovici *et al.* Ligo: The laser interferometer gravitational wave observatory. *Science*, 256:325, 1992.

[2] Ramesh Narayan, Bohdan Paczynski, and Tsvi Piran. Gamma-ray bursts as the death throes of massive binary stars. *Astrophys. J.*, 395:L83, 1992. astro-ph/9204001.

- [3] N. Gehrels *et al.* A short γ -ray burst apparently associated with an elliptical galaxy at redshift $z = 0.225$. *Nature (London)*, 437:851–854, October 2005.
- [4] W. H. Lee, E. Ramirez-Ruiz, and J. Granot. A Compact Binary Merger Model for the Short, Hard GRB 050509b. *Astrophys. J. Lett.*, 630:L165–L168, September 2005.
- [5] A. et al. Rau. Exploring the Optical Transient Sky with the Palomar Transient Factory. *PASP*, 121:1334–1351, December 2009.
- [6] N. Kaiser. Pan-STARRS: a wide-field optical survey telescope array. In J. M. Oschmann Jr., editor, *Society of Photo-Optical Instrumentation Engineers (SPIE) Conference Series*, volume 5489 of *Society of Photo-Optical Instrumentation Engineers (SPIE) Conference Series*, pages 11–22, October 2004.
- [7] LSST Science Collaborations, P. A. Abell, J. Allison, S. F. Anderson, J. R. Andrew, J. R. P. Angel, L. Armus, D. Arnett, S. J. Asztalos, T. S. Axelrod, and et al. LSST Science Book, Version 2.0. *ArXiv e-prints*, December 2009.
- [8] B. D. Metzger and E. Berger. What is the Most Promising Electromagnetic Counterpart of a Neutron Star Binary Merger? *ArXiv e-prints*, August 2011.
- [9] Branson C. Stephens, William E. East, and Frans Pretorius. Eccentric Black Hole-Neutron Star Mergers. *Astrophys. J. Lett.*, 737(1):L5, 2011.
- [10] R. Gold, S. Bernuzzi, M. Thierfelder, B. Bruegmann, and F. Pretorius. Eccentric binary neutron star mergers. *ArXiv e-prints*, September 2011.
- [11] Masaru Shibata and Keisuke Taniguchi. Coalescence of black hole-neutron star binaries. *Living Reviews in Relativity*, 14(6), 2011.
- [12] R. M. O’Leary, B. Kocsis, and A. Loeb. Gravitational waves from scattering of stellar-mass black holes in galactic nuclei. *Mon. Not. Roy. Astron. Soc.*, 395:2127–2146, June 2009.
- [13] W. H. Lee, E. Ramirez-Ruiz, and G. van de Ven. Short Gamma-ray Bursts from Dynamically Assembled Compact Binaries in Globular Clusters: Pathways, Rates, Hydrodynamics, and Cosmological Setting. *Astrophys. J.*, 720:953–975, September 2010.
- [14] J. Grindlay, S. Portegies Zwart, and S. McMillan. Short gamma-ray bursts from binary neutron star mergers in globular clusters. *Nature Physics*, 2:116–119, February 2006.
- [15] R. Salvaterra, A. Cerutti, G. Chincarini, M. Colpi, C. Guidorzi, and P. Romano. Short Gamma-ray bursts: a bimodal origin? *Mon. Not. Roy. Astron. Soc.*, 388:L6–L9, July 2008.
- [16] D. Guetta and L. Stella. Short γ -ray bursts and gravitational waves from dynamically formed merging binaries. *Astron. and Astrophys.*, 498:329–333, May 2009.
- [17] B. Kocsis and J. Levin. Repeated Bursts from Relativistic Scattering of Compact Objects in Galactic Nuclei. *ArXiv e-prints*, September 2011.
- [18] E. Berger. A Short Gamma-ray Burst ”No-host” Problem? Investigating Large Progenitor Offsets for Short GRBs with Optical Afterglows. *Astrophys. J.*, 722:1946–1961, October 2010.
- [19] R. P. Church, A. J. Levan, M. B. Davies, and N. Tanvir. Implications for the origin of short gamma-ray bursts from their observed positions around their host galaxies. *Mon. Not. Roy. Astron. Soc.*, pages 355–+, March 2011.
- [20] J. D. M. Dewi, P. Podsiadlowski, and O. R. Pols. The spin period-eccentricity relation of double neutron stars: evidence for weak supernova kicks? *Mon. Not. Roy. Astron. Soc.*, 363:L71–L75, October 2005.
- [21] J. P. Norris, N. Gehrels, and J. D. Scargle. Heterogeneity in Short Gamma-Ray Bursts. *Astrophys. J.*, 735:23, July 2011.
- [22] W. F. Domainko. Finding short GRB remnants in globular clusters: the VHE gamma-ray source in Terzan 5. *Astron. and Astrophys.*, 533:L5, September 2011.
- [23] T. A. Thompson. Accelerating Compact Object Mergers in Triple Systems with the Kozai Resonance: A Mechanism for ”Prompt” Type Ia Supernovae, Gamma-Ray Bursts, and Other Exotica. *Astrophys. J.*, 741:82, November 2011.
- [24] Linqing Wen. On the Eccentricity Distribution of Coalescing Black Hole Binaries Driven by the Kozai Mechanism in Globular Clusters. *Astrophys. J.*, 598:419–430, 2003.
- [25] Charles F. Gammie, Stuart L. Shapiro, and Jonathan C. McKinney. Black Hole Spin Evolution. *Astrophys. J.*, 602:312–319, 2004.
- [26] J. M. Miller, M. C. Miller, and C. S. Reynolds. The Angular Momenta of Neutron Stars and Black Holes as a Window on Supernovae. 2011.
- [27] Z. B. Etienne, Y. T. Liu, S. L. Shapiro, and T. W. Baumgarte. General relativistic simulations of black-hole-neutron-star mergers: Effects of black-hole spin. *Phys. Rev. D*, 79(4):044024, 2009.
- [28] Francois Foucart, Matthew D. Duez, Lawrence E. Kidder, and Saul A. Teukolsky. Black hole-neutron star mergers: effects of the orientation of the black hole spin. *Phys. Rev.*, D83:024005, 2011.
- [29] Koutarou Kyutoku, Hirotda Okawa, Masaru Shibata, and Keisuke Taniguchi. Gravitational waves from spinning black hole-neutron star binaries: dependence on black hole spins and on neutron star equations of state. *Phys. Rev.*, D84:064018, 2011.
- [30] Sarvnipun Chawla et al. Mergers of Magnetized Neutron Stars with Spinning Black Holes: Disruption, Accretion and fallback. *Phys. Rev. Lett.*, 105:111101, 2010.
- [31] J. S. Read, C. Markakis, M. Shibata, K. Uryū, J. D. E. Creighton, and J. L. Friedman. Measuring the neutron star equation of state with gravitational wave observations. *Phys. Rev. D*, 79(12):124033, 2009.
- [32] M. Shibata and K. Uryū. Merger of black hole-neutron star binaries: Nonspinning black hole case. *Phys. Rev. D*, 74(12):121503, 2006.
- [33] Matthew D. Duez, Francois Foucart, Lawrence E. Kidder, Christian D. Ott, and Saul A. Teukolsky. Equation of state effects in black hole-neutron star mergers. *Class. Quant. Grav.*, 27:114106, 2010.
- [34] Francesco Pannarale, Luciano Rezzolla, Frank Ohme, and Jocelyn S. Read. Will black hole-neutron star binary inspirals tell us about the neutron star equation of state? 2011.
- [35] K. Kyutoku, M. Shibata, and K. Taniguchi. Gravitational waves from nonspinning black hole-neutron star binaries: Dependence on equations of state. *Phys. Rev. D*, 82(4):044049–+, August 2010.
- [36] Benjamin D. Lackey, Koutarou Kyutoku, Masaru Shibata, Patrick R. Brady, and John L. Friedman. Extracting equation of state parameters from black hole-neutron star mergers. I. Nonspinning black holes. 2011.

- [37] S. Chawla, M. Anderson, M. Besselman, L. Lehner, S. L. Liebling, P. M. Motl, and D. Neilsen. Mergers of Magnetized Neutron Stars with Spinning Black Holes: Disruption, Accretion and Fallback. *ArXiv e-prints*, 2010.
- [38] F. Foucart, M. D. Duez, L. E. Kidder, M. A. Scheel, B. Szilagyi, and S. A. Teukolsky. Black hole-neutron star mergers for 10 solar mass black holes. *ArXiv e-prints*, November 2011.
- [39] William E East, Frans Pretorius, and Branson C Stephens. 2011. in prep.
- [40] F. Löffler, L. Rezzolla, and M. Ansorg. Numerical evolutions of a black hole-neutron star system in full general relativity: Head-on collision. *Phys. Rev. D*, 74(10):104018, 2006.
- [41] H. Friedrich. On the hyperbolicity of Einstein's and other gauge field equations. *Communications in Mathematical Physics*, 100:525–543, December 1985.
- [42] D. Garfinkle. Harmonic coordinate method for simulating generic singularities. *Phys. Rev. D*, 65(4):044029, 2002.
- [43] F. Pretorius. Numerical relativity using a generalized harmonic decomposition. *Class. and Quant. Grav.*, 22:425, 2005.
- [44] Carsten Gundlach, Jose M. Martin-Garcia, Gioel Calabrese, and Ian Hinder. Constraint damping in the Z4 formulation and harmonic gauge. *Class. Quant. Grav.*, 22:3767–3774, 2005.
- [45] F. Pretorius. Evolution of Binary Black-Hole Spacetimes. *Phys. Rev. Lett.*, 95(12):121101, 2005.
- [46] Matthew W. Choptuik and Frans Pretorius. Ultra Relativistic Particle Collisions. *Phys. Rev. Lett.*, 104:111101, 2010.
- [47] Lee Lindblom and Bela Szilagyi. An Improved Gauge Driver for the GH Einstein System. *Phys. Rev.*, D80:084019, 2009.
- [48] A. Harten, P.D. Lax, and B.J. van Leer. *SIAM Rev.*, 25:35, 1983.
- [49] A. Tchekhovskoy, J. C. McKinney, and R. Narayan. WHAM: a WENO-based general relativistic numerical scheme - I. Hydrodynamics. *Mon. Not. Roy. Astron. Soc.*, 379:469, 2007.
- [50] Marsha J Berger and Joseph Olinger. Adaptive mesh refinement for hyperbolic partial differential equations. *Journal of Computational Physics*, 53(3):484, 1984.
- [51] M.J. Berger and P. Colella. Local adaptive mesh refinement for shock hydrodynamics. *Journal of Computational Physics*, 82(1):64, 1989.
- [52] G. D. Quinlan and S. L. Shapiro. The collapse of dense star clusters to supermassive black holes - Binaries and gravitational radiation. *Astrophys. J.*, 321:199–210, October 1987.
- [53] M. Turner. Gravitational radiation from point-masses in unbound orbits - Newtonian results. *Astrophys. J.*, 216:610–619, 1977.
- [54] Paul Demorest, Tim Pennucci, Scott Ransom, Mallory Roberts, and Jason Hessels. Shapiro delay measurement of a two solar mass neutron star. *Nature*, 467:1081–1083, 2010.
- [55] M. J. Rees. Tidal disruption of stars by black holes of 10 to the 6th-10 to the 8th solar masses in nearby galaxies. *Nature (London)*, 333:523–528, June 1988.
- [56] W. Kastaun, B. Willburger, and K. D. Kokkotas. Saturation amplitude of the f-mode instability. *Phys. Rev. D*, 82(10):104036, November 2010.
- [57] Christopher P. L. Berry and Jonathan R. Gair. Gravitational wave energy spectrum of a parabolic encounter. *Phys. Rev.*, D82:107501, 2010.
- [58] K. Glampedakis and D. Kennefick. Zoom and whirl: Eccentric equatorial orbits around spinning black holes and their evolution under gravitational radiation reaction. *Phys. Rev. D*, 66(4):044002, 2002.
- [59] Neil J. Cornish and Janna J. Levin. Lyapunov timescales and black hole binaries. *Class. Quant. Grav.*, 20:1649–1660, 2003.
- [60] Frans Pretorius and Deepak Khurana. Black hole mergers and unstable circular orbits. *Class. Quant. Grav.*, 24:S83–S108, 2007.
- [61] P.C. Peters and J. Mathews. Gravitational Radiation from Point Masses in a Keplerian Orbit. *Phys. Rev.*, 131:435–440, 1963.